AMERICAN SOCIETY FOR MICROBIOLOGY | Infection and Immunity®

FUNGAL AND PARASITIC INFECTIONS

Single-Cell Heterogeneity of the Liver-Infiltrating Lymphocytes in Individuals with Chronic *Echinococcus multilocularis* Infection

Tiemin Jiang,[a] Wujianan Sun,[b] Tuerganaili Aji,[c] Yingmei Shao,[c] Chuang Guo,[b] Chuanshan Zhang,[a] Bo Ran,[c] Jiao Hou,[a] Aimaiti Yasen,[a] Qiang Guo,[c] Hui Wang,[a] Kun Qu,[b,d] Hao Wen[a,c]

[a]State Key Laboratory of Pathogenesis, Prevention and Management of High Incidence Diseases in Central Asia, The First Affiliated Hospital of Xinjiang Medical University, Urumqi, Xinjiang, China

[b]Department of Oncology, The First Affiliated Hospital of USTC, School of Basic Medical Sciences, Division of Life Sciences and Medicine, University of Science and Technology of China, Hefei, Anhui, China

[c]Department of Hepatobiliary and Echinococcosis Surgery, Digestive and Vascular Surgery Center, The First Affiliated Hospital of Xinjiang Medical University, Urumqi, Xinjiang, China

[d]School of Data Science, University of Science and Technology of China, Hefei, China

Tiemin Jiang and Wujianan Sun contributed equally to this work. Author order was determined alphabetically.

ABSTRACT Human alveolar echinococcosis (AE) is a tumor-like disease predominantly located in the liver. The cellular composition and heterogeneity of the lesion-infiltrating lymphocytes which produce an "immunosuppressive" microenvironment are poorly understood. Here, we profiled 83,921 CD45$^+$ lymphocytes isolated from the peripheral blood (PB), perilesion (PL), and adjacent normal (AN) liver tissue of four advanced-stage AE patients using single-cell RNA and T-cell receptor (TCR) sequencing technology. We identified 23 large clusters, and the distributions and transcriptomes of these cell clusters in the liver and periphery were different. The cellular proportions of exhausted CD8$^+$ T cells and group 2 innate lymphoid cells (ILC2s) were notably higher in PL tissue, and the expression features of these cell subsets were related to neoplasm metastasis and immune response suppression. In the 5 CD8$^+$ T-cell populations, only CD8$^+$ mucosa-associated invariant T (MAIT) cells were enriched in PL samples and the TRAV1-2_TRAJ33_TRAC TCR was clonally expanded. In the 11 subsets of CD4$^+$ T cells, Th17 cells and induced regulatory T cells (iTregs) were preferentially enriched in PL samples, and their highly expressed genes were related to cell invasion, tumor metastasis, and inhibition of the inflammatory immune response. Exhaustion-specific genes (TIGIT, PD-1, and CTLA4) were upregulated in Tregs. Interestingly, there was a close contact between CD8$^+$ T cells and iTregs or Th17 cells, especially for genes related to immunosuppression, such as PDCD1-FAM3C, which were highly expressed in PL tissue. This transcriptional data set provides valuable insights and a rich resource for deeply understanding the immune microenvironment in AE, which could provide potential target signatures for AE diagnosis and immunotherapies.

KEYWORDS alveolar echinococcosis, *Echinococcus multilocularis*, immune microenvironment, infiltrating lymphocytes, heterogeneity, single-cell sequencing

Human alveolar echinococcosis (AE) is a potentially lethal helminthic disease that is caused by infection with the metacestode, or larval stage, of the cestode *Echinococcus multilocularis* in the Northern Hemisphere (1). A systematic search of the global literature on the epidemiology of human AE showed the increasing spread of reported cases and the rise in case numbers in the 21st century, especially in western, northern, and eastern Europe, as well as in central Asia (2). Annually, more than 18,000 new AE cases are estimated to occur worldwide, with 91% of them occurring in China (3). Human AE primarily

Editor De'Broski R. Herbert, University of Pennsylvania

Address correspondence to Hui Wang, wangh0923@126.com, Kun Qu, qukun@ustc.edu.cn, or Hao Wen, dr.wenhao@163.com.

The authors declare no conflict of interest.

Received 29 April 2022
Returned for modification 14 June 2022
Accepted 16 September 2022

occurs in the liver, which shows tumor-like malignant growth of the *E. multilocularis* metacestode that frequently results in invasion and destruction in the liver and other host organs (4). Due to its aggressive growth, AE leads to death in 90% of infected individuals within 10 to 15 years of diagnosis if left untreated (5). Thus, increased understanding of the immune mechanisms of pathology and protection of *E. multilocularis* infection in order to search for other treatment methods is urgently needed.

Some clinical observations have revealed that the type of immune response elicited in the host determines the outcome of *E. multilocularis* larval infection. Observations in hosts with impaired immunity, such as in the context of AIDS, organ transplantation, or cancer chemotherapy, strongly suggest that immunosuppression increases disease severity, leading to uncontrolled proliferation of the metacestode (6). In fact, the survival of *E. multilocularis* larvae in the host relies upon their ability to create an "immunosuppressive" microenvironment, leading to a kind of balance between the parasite and host to maintain immune homoeostasis during persistent infection (7). The metacestode continuously proliferates and infiltrates, thus forming a growing hepatic lesion that consists of a large conglomerate of parasite vesicles, which are intermingled with mainly host connective tissue and infiltrating immune cells. Recently, histopathological analysis of human AE liver samples showed that the immune infiltrate around liver lesions was composed of macrophages, lymphocytes, granulocytes, and myofibroblasts. Among these cells, large clusters of $CD4^+$ T cells and $CD8^+$ T cells were found to accumulate around the metacestode in the liver (8). The progressive clinical course of AE is associated with significant specific stimulation of T cells, leading to the disruption of T-cell signaling and T-cell exhaustion in the late stage of infection (9). Our recent study showed that the coinhibitory receptor T-cell immunoglobulin and immunoreceptor tyrosine-based inhibitory motif domain (TIGIT), which is known to limit T-cell function, was an enriched gene in a heatmap generated by comparing mRNA arrays of paired AE liver tissues (8). Flow cytometric analysis further confirmed that the absolute numbers of $TIGIT^+$ $CD4^+$ T cells and $TIGIT^+$ $CD8^+$ T cells in paired liver tissue samples were significantly higher in perilesion (PL) tissue than in adjacent normal (AN) tissue and that the hepatic infiltrating $TIGIT^+$ $CD4^+$ T cells and $TIGIT^+$ $CD8^+$ T cells had lower expression of granzyme B, perforin, interferon gamma (IFN-γ), and tumor necrosis factor alpha (TNF-α) in PL tissue than in AN tissue, suggesting an "exhausted" parasite-induced T-cell response (8). In addition, persistent infection has been reported to be mediated by specialized regulatory T cells (Tregs) and related cytokines, such as interleukin-10 (IL-10) and transforming growth factor β (TGF-β) (10, 11). These cells may contribute to the production of the "immunosuppressive" microenvironment that leads to the maintenance of *E. multilocularis* survival. However, the systematic cellular composition and functional heterogeneity of lesion-infiltrating lymphocytes in the hepatic AE lesion microenvironment are currently poorly understood. Therefore, a deep understanding of the profile of infiltrating immune cells in hepatic AE microenvironments will provide better strategies to modulate the immune system to eradicate *E. multilocularis*.

Single-cell RNA sequencing (scRNA-seq) is a powerful tool for defining cell types and states on the basis of individual cell transcriptomes in health and disease (12). Recently, scRNA-seq has been applied to analyze infiltrating lymphocytes from cancer patients (13, 14) and cystic echinococcosis (CE) patients (15), allowing a detailed understanding of the dynamic nature of these infiltrating cells in the highly complex cancer or parasite microenvironment. In addition, scRNA-seq provides an advanced method to define T-cell receptor (TCR) sequences for each cell (16). In this study, we performed scRNA-seq analysis of 81,865 single $CD45^+$ lymphocytes isolated from the peripheral blood (PB), PL tissue, and paired AN liver tissue of four hepatic AE patients to identify the infiltrating immune cells and their complete TCR sequences in the lesion microenvironment. We identified 23 cell subsets with distinct tissue distribution patterns, including novel cell subsets such as group 2 innate lymphoid cells (ILC2s) and mucosa-associated invariant T (MAIT) cells. The signature genes for exhausted $CD8^+$ T cells,

MAIT cells, ILC2s, and Tregs were examined in detail. Our results provide a valuable resource for studying the basic characteristics of immune cells in the AE microenvironment and potentially guiding effective immunotherapeutic strategies.

RESULTS

Infiltrating immune cells in the hepatic AE tissue microenvironment. To characterize the immune cell profiles in AE, we applied scRNA-seq and single-cell TCR sequencing (scTCR-seq) methods to study CD45$^+$ cells isolated from PB, PL liver tissue, and AN liver tissue samples from four AE patients (Fig. 1a). All of the patients had biologically active AE lesions that were evidenced by computed tomography (CT) or magnetic resonance imaging (MRI) scans and histopathological analysis (see Fig. S1A in the supplemental material). Hematoxylin and eosin (H&E) staining showed typical parasitic material inside lesions formed by *E. multilocularis* metacestodes, including many small, polymorphous, and partly conglomerated cysts, and contorted parts of the laminated layer were present in the lumina of some of the cysts with a rather reddish appearance (Fig. S1B). The baseline clinical characteristics of the 4 AE patients studied are shown in Table S1. After quality control, we obtained a total of 83,921 cells from 11 samples, with an average of 1,602 genes detected per cell (Fig. S2A). Seurat was used to integrate all the samples, and 23 subgroups were obtained through an unsupervised clustering method using marker genes (Fig. 1b and c; Fig. S2B and C) (17). These subgroups included B cells, plasma cells, four CD4$^+$ T-cell clusters including activated CD4$^+$ T cells (TCF7), naive CD4$^+$ T cells (LEF1), cytotoxic CD4$^+$ T cells (CX3CR1 and FGFBP2), and CD4$^+$ Tregs (FOXP3 and CTLA4), four CD8$^+$ T-cell clusters including naive CD8$^+$ T cells (CCR7 and SELL), effector CD8$^+$ T cells (CD69), exhausted CD8$^+$ T cells (PDCD1) (18), and CD8$^+$ MAIT cells (RORC), phosphoantigen-reactive $\gamma\delta$ T (PRGDT) cells (PRGDT), two innate lymphoid cell (ILC) clusters including group 1 ILCs (ILC1s) (LAG3) and ILC2s (GFI1 and IL-4), four natural killer (NK) cell clusters, two monocyte (CD14$^+$ and FCGR3A$^+$) clusters, dendritic cells (DCs), plasmacytoid DCs (pDCs, IL3RA), and platelets (Fig. 1d). The 23 cell clusters were all identified in the three tissues, and the presence of cells from each patient in each subgroup indicated that the data were highly reproducible. However, there were some differences in the source of cells in each subgroup, indicating immune profile changes among the PL, AN, and PB samples (Fig. 1d).

Changes in the immune cell landscape of the AE tissue microenvironment. To describe the changes in the immune cell profiles among the PL, AN, and PB samples in detail, we analyzed the source of each cell type for each patient (Fig. S3A) and then compared the differences among the three sources (Fig. S3B). When comparing PL and AN liver tissues with the PB, we found that the changes in the immune profile mainly showed the difference between the liver and the periphery, and the patients exhibited the same trends, such as the proportions of B cells, plasma cells, CD4_naive cells, CD8_effector cells, CD8_naive cells, and monocytes being increased in the PB, while those of PRGDT cells, NK cells, ILCs, pDCs, and especially CD8_exhaustion cells were enriched in the liver tissues (PL and AN samples) (Fig. 2a and b). Disease enrichment analysis found that the differentially expressed genes (DEGs) of CD8_exhaustion cells in the PL high group showed enrichment of the disease term "immunosuppression" (Fig. 2d), suggesting that exhausted CD8$^+$ T cells play an immunosuppressive role in the AE microenvironment favoring persistent *E. multilocularis* infection, which is consistent with our recent findings (8).

As comparing PL and AN liver tissues could better reflect the changes in the immune response in the AE tissue microenvironment, we then performed an analysis to determine which cell types in the liver had a tendency to accumulate in the PL region. We analyzed the differences between PL and AN tissues for each cell type, calculated the patient consistency, and found that the proportions of CD4_naive cells, CD8_naive cells, CD4_cytotoxic cells, NK_NCAM1 cells, NKT2 cells, ILC1s, and CD8_effector cells in the PL site were decreased, while Mono_CD14 cells, NKT1 cells, CD4_Tregs, MAIT cells, DCs, pDCs, B cells, PRGDT cells, CD8_exhaustion cells, and ILC2s were enriched in the PL site (Fig. 2c; Fig. S3B).

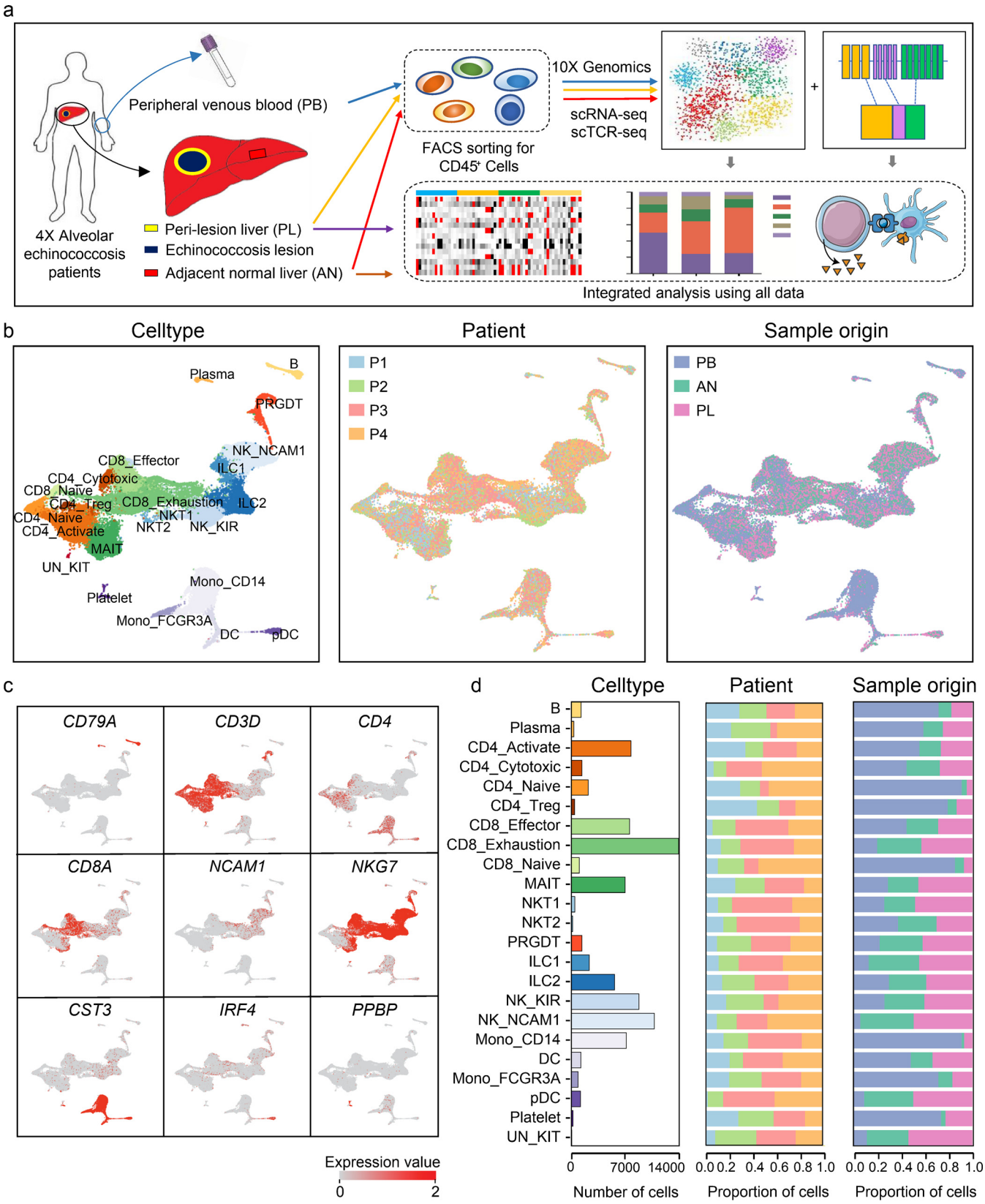

FIG 1 Single-cell landscape of peripheral blood and liver biopsy specimens from alveolar echinococcosis patients. (a) Flowchart depicting the overall design of the study. FACS, fluorescence-activated cell sorter. (b) Uniform manifold approximation and projection (UMAP) visualization of scRNA-seq data for single cells derived from AE patients. Cells were color coded by cell type (left), patient (middle), or sample origin (right); each dot represents one cell. DC, dendritic cells; pDCs, plasmacytoid dendritic cells; Mono, monocyte; NK, natural killer cells; MAIT, mucosa-associated invariant T cells; ILC, innate lymphoid

(Continued on next page)

Interestingly, among the cell types at the PL site, ILC2s showed the highest patient consistency.

We next performed a pairwise comparison of the three sources of ILC2s followed by unsupervised clustering of the DEGs to obtain five groups (liver PL high, liver AN high, PL high, PB high, and AN high) (Fig. 2e). We found that the liver PL high and liver AN groups included genes such as *CXCR4*, *ZBTB16*, and *HLA-G*, which mainly reflected the difference between the liver and PB. Strikingly, tumor-related genes such as *IFNG*, *ANXA1*, *FOSB*, and *HSPA90AA1* were highly expressed in the PL region. Disease enrichment analysis also found that the DEGs in the PL high group showed enrichment of the disease terms "hepatic neoplasms" and "neoplasm metastasis." The DEGs in the AN high group were enriched in only liver cirrhosis (Fig. 2f). Gene ontology (GO) enrichment analysis found that the DEGs in the PL high and PB high groups were enriched in the "apoptotic signaling pathway," "leukocyte activation," and "NK cell-mediated cytotoxicity" (Fig. 2g). The DEGs of the three groups were all enriched in cytokine-mediated signaling pathways (Fig. 2g). Therefore, we conducted a differential analysis of all cytokines and found that genes such as *CCL4L2*, *IFNG*, and *TNF* were highly expressed in the PB and PL site (Fig. 2h). These results suggested that these genes might promote the development and metastasis of AE lesions, which could explain why AE exhibits malignant tumor-like symptoms and metastasis.

CD8$^+$ T-cell subtype analysis in the hepatic AE tissue microenvironment. CD8$^+$ T cells mainly play a cytotoxic role in the immune response (19). To reveal the potential functional subtypes of CD8$^+$ T cells, we performed a comparison between PL and AN liver tissues to determine which CD8$^+$ T-cell subsets in the liver exhibited a tendency to accumulate in the PL site. We found that only MAIT cells were enriched in PL tissue (Fig. 3a and b). Therefore, we conducted a differential analysis of MAIT cells and found that genes related to cell killing and cytokine secretion, such as *GZMA* and *CXCR6*, were highly expressed in cells in AN tissue. PL highly expressed *MYADM*, *FOS*, *LMNA*, and other tumor-related genes (Fig. 3c). Disease enrichment analysis also found that the DEGs highly expressed in PL tissue were enriched in the terms "neoplastic cell transformation" and "lung neoplasms and carcinoma" (Fig. 3d). GO term enrichment analysis of the DEGs highly expressed in PL tissues identified enrichment in "negative regulation of cytokine production," "apoptotic signaling pathway," "positive regulation of cell migration," and "regulation of extracellular matrix assembly" (Fig. 3e). These terms indicate that the AE tissue microenvironment has functions related to suppressing the immune response and promoting apoptosis and cell migration, which further explains why AE patients exhibit severe pathological damage to the liver and growth with a malignant tumor-like pattern.

More importantly, we found that the DEGs that were highly expressed in PL tissue were enriched in the inflammatory response to antigenic stimuli (Fig. 3e). To determine the receptors that respond to parasite antigens in AE patients, we performed scTCR-seq and found that in MAIT cells from all patients, the TRAV1-2_TRAJ33_TRAC TCR exhibited significant clonal expansion in PL tissue but that in other cell types, the patients did not exhibit clonal expansion of common TCRs (Fig. 3f; Fig. S4). The proportion of MAIT cells carrying the TRAV1-2_TRAJ33_TRAC TCR showed an increasing trend among the PB, AN liver tissue, and PL liver tissue (Fig. 3g). Therefore, we speculated that this TCR may respond to some of the parasite antigens and that vaccines based on this receptor are expected to prevent the occurrence of AE in patients.

CD4$^+$ T-cell subtype analysis in the hepatic AE tissue microenvironment. Because it is well established that not only CD8$^+$ T cells but also CD4$^+$ T cells are critical for controlling metacestode growth in the liver (7, 8), we reclustered all CD4$^+$ T cells

FIG 1 Legend (Continued)

cells; Treg, regulatory T cells; NKT, natural killer T cells; PRGDT, phosphoantigen-reactive $\gamma\delta$ T cells; UN_KIT, unknown. (c) Expression patterns of marker genes used for cell type annotation. The expression levels of marker genes are indicated by color. (d) For each of the 23 cell subclusters, the number of cells, the proportion of cells originating from each of the four patients, and the proportion of cells originating from each of the three tissues are shown from left to right, respectively. The left column indicates the cell subtypes identified based on combinations of marker genes.

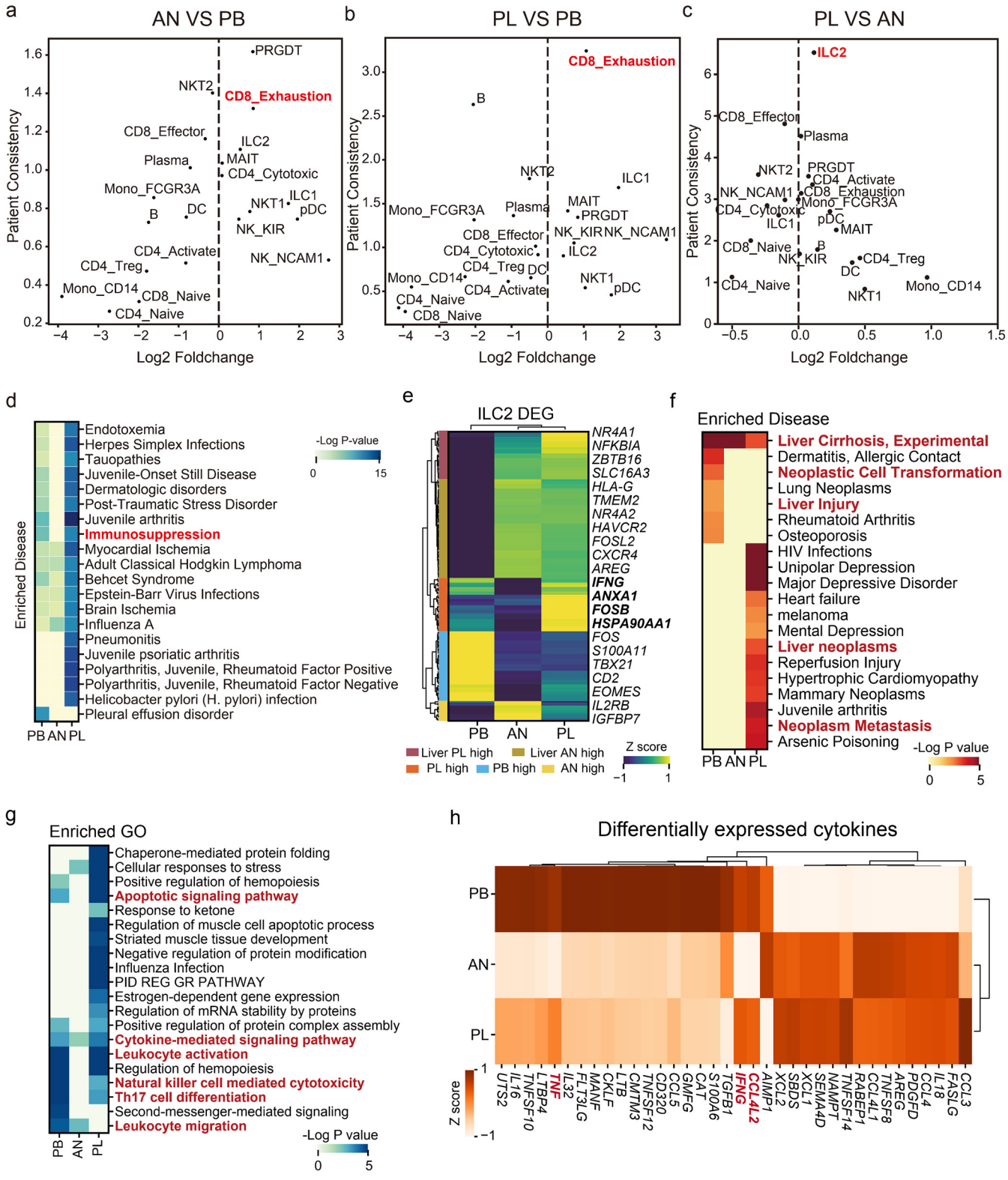

FIG 2 Exhausted CD8$^+$ T cells and ILC2s are enriched in the PL and AN tissues of AE patients. (a to c) Differences in the proportions of cells among all cells and consistency in the differences between AN and PB (a), PL and PB (b), and PL and AN (c) samples across the patients. ILC2s (c) and exhausted CD8$^+$ T cells (a and b) are marked red because there were higher proportional changes in these cells in the PL site than in the AN site (c), in the AN site than in the PB (a), or in the PL site than in the PB (b). (d) Heatmap showing the enriched diseases for genes differentially expressed in exhausted CD8$^+$ T cells among PB, AN, and PL samples. *P* values were calculated using Student's *t* test. Diseases related to the immune response are marked in bold red text. (e) Heatmap of the differentially expressed genes of ILC2s in PB, AN, and PL samples. The genes were clustered by unsupervised clustering. The means of the expression levels of the differentially expressed genes are indicated by color. (f) Heatmap showing the enriched diseases for genes differentially expressed

(Continued on next page)

and obtained a total of 11 subclusters (Fig. 4a). According to the expression of marker genes, these cells could be defined as naive cells, Th1 cells, Th2 cells, Th17 cells, induced Tregs (iTregs), naive Tregs (nTregs), cytotoxic cells, and some $CD8^+$ cells mixed in due to clustering errors (Fig. 4a and b; Fig. S5). Similarly, we found that there were differences in the cell source for each cell type, and the source of each cell type was heterogeneous among the patients (Fig. S5D and S6A). For example, most of the naive_8 cells were derived from the PB of P1, and the proportion of cells derived from the PB of P3 was significantly reduced (Fig. S6A).

To describe the changes in $CD4^+$ T cells in the AE patients, we compared the proportions of cells derived from PL liver tissue, AN liver tissue, and the PB for each $CD4^+$ cell type. We found that the PL and AN liver tissues had the same trends for changes as the PB (Fig. S6B and C). For example, the proportions of cytotoxic cells, Th1 cells, and iTregs were enriched in the PL and AN liver tissues, while the proportions of naive cells, Th2 cells, and nTregs were increased in the PB, which also reflected the difference between the liver and periphery (Fig. S6B and C). To investigate the $CD4^+$ cell changes in the AE tissue microenvironment in detail, we compared the differences between PL and AN liver tissues and calculated the fold change in each cell type and the associated patient consistency (Fig. 4c; Fig. S6D). We found that the proportions of Th1 cells, naive cells, and cytotoxic cells in the PL site were reduced but that those of exhaustion-related iTregs, Th17 cells, and nTregs were significantly increased in the PL site compared to the AN site (Fig. 4c). Additionally, Th17 cells and iTregs had high patient consistency, which indicates that the AE tissue microenvironment is in a state of immunosuppression.

We further analyzed the expression of exhaustion-related genes in $CD4^+$ T cells from PB, AN, and PL samples and found that iTregs had higher expression of most of the exhaustion-related genes (*CTLA4*, *LAG3*, *PDCD1*, and *HAVCR2*) than other $CD4^+$ T-cell subsets (Fig. 4d). Interestingly, we performed a differential analysis of Th17 cells and showed the expression of DEGs in PL and AN liver tissues (Fig. 4e). We found that *TSC22D3*, *MCL1*, and other genes related to the inhibition of inflammation and the immune response were highly expressed in PL tissue (20) (Fig. 4e). GO enrichment analysis also found that PL tissue highly expressed DEGs enriched in apoptosis-related GO terms, further indicating that the AE tissue microenvironment was in a state of immunosuppression (Fig. 4e and f). Differential analysis of iTregs revealed that oncogenes such as *SET* and *OCIAD2* were highly expressed in PL tissue and that *SEC11A*, which promotes cell invasion and tumor metastasis, was especially enriched (21) (Fig. 4g). Genes with antimicrobial activity, such as *LGALS3*, were highly expressed in AN tissue (22) (Fig. 4g). GO enrichment analysis also found that DEGs with high PL expression were enriched in GO terms such as "nonalcoholic fatty liver disease (NAFLD)" (Fig. 4h), which might explain the severe parenchymal damage caused by AE.

Interactions of iTregs and Th17 cells with $CD8^+$ T cells. Tregs, Th17 cells, and $CD8^+$ T cells are all key immunomodulators in AE (8, 11). Thus, the regulatory relationships between $CD8^+$ T cells and Th17 cells or iTregs were separately analyzed using immune-related ligand-receptor pairs (23). Focusing on the interaction between Th17 and $CD8^+$ T cells, the receptor-ligand pairs enriched in both the PB and the AN and PL liver tissues included CD47-SIRPG, which is related to T-cell activation (24), and CD48-CD244, which is related to T-cell immunosuppression (25) (Fig. S7A). The receptor-ligand pairs enriched in AN and PL liver tissues included CXCR3-CCL20 and CCR6-CCL20, which regulate the migration of Th17 cells to local tissues (26), LGALS9-CD47, LGALS9-CD44, and PDCD1-FAM3C, which have been reported to be related to

FIG 2 Legend (Continued)
in ILC2s in PB, AN, and PL samples. *P* values were calculated using Student's *t* test. Diseases related to the immune response are marked in bold red text. (g) Heatmap showing the enriched GO terms for genes differentially expressed in ILC2s in PB, AN, and PL samples. *P* values were calculated using Student's *t* test. GO terms related to the immune response are marked in bold red text. (h) Heatmap of the differentially expressed cytokine genes of ILC2s in PB, AN, and PL samples. Genes were clustered by unsupervised clustering. The means of the expression levels of the differentially expressed genes are indicated by color.

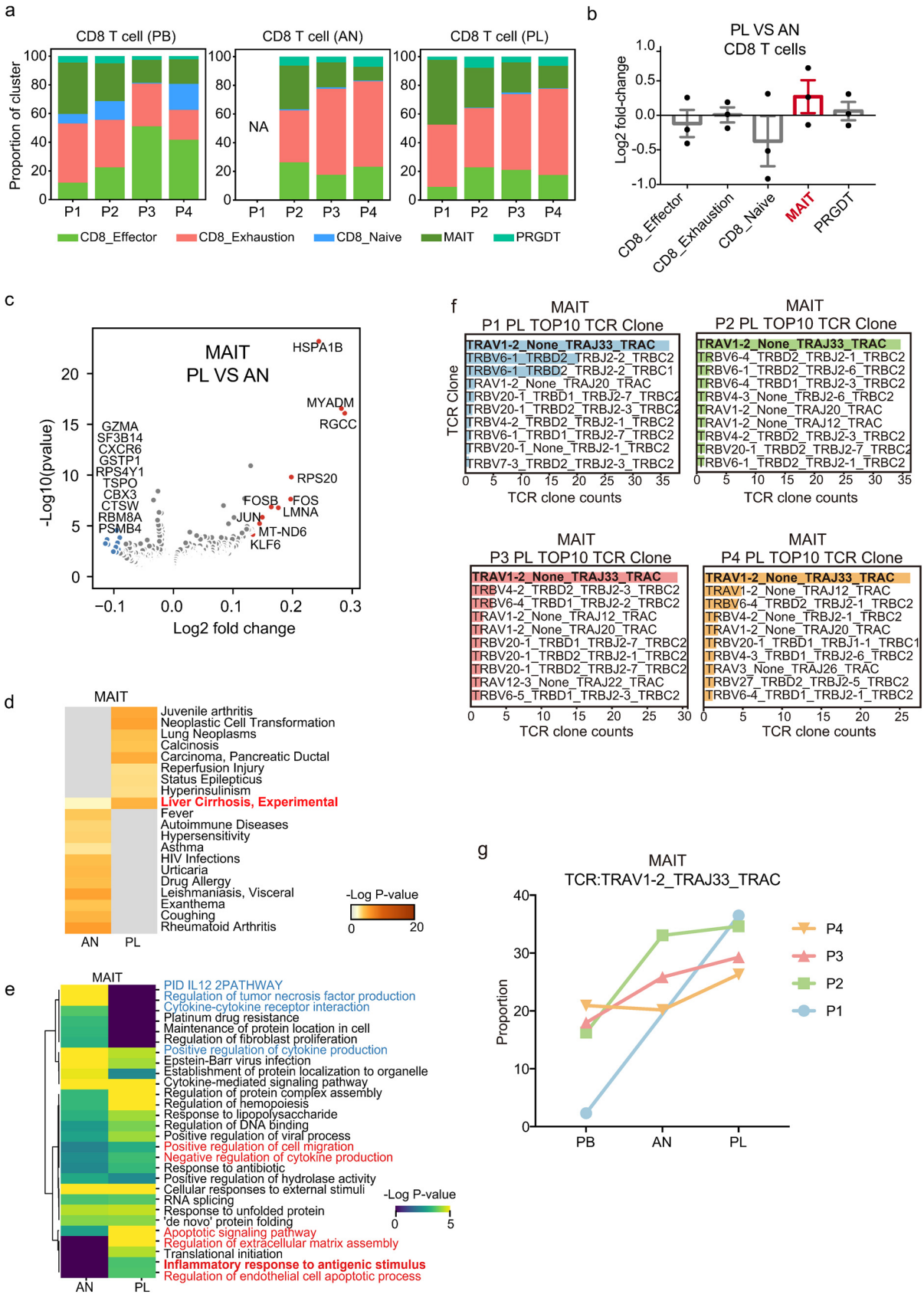

FIG 3 TCR analysis identified a significantly expanded MAIT cell clone correlated with cell dysfunction in PL tissue. (a) Percentages of CD8$^+$ T-cell subtypes in the PB, AN, and PL samples from the patients. (b) Differences in the proportions of cells among CD8$^+$ T cells

(Continued on next page)

immunosuppression (27), *TNF* and its receptors *ICOS*, *TNFRF1B*, and *FAS*, and apoptosis-related FAS-FASLG (28) (Fig. 5a), which was also consistent with the enrichment of the GO term "apoptosis" in Th17 cells in PL and AN liver tissues (Fig. 4f). For the interaction between iTregs and $CD8^+$ T cells, the receptor-ligand pairs enriched in both the PB and the AN and PL tissues included CD40LG-a5b1 complex, which is related to costimulation of T cells (29), and LGALS9-CD47, which is related to T-cell immunosuppression (27) (Fig. 5b). The receptor-ligand pairs enriched in AN and PL tissues included CXCR6-CXCL16, CXCR3-CCL20, and CCR6-CCL20, which regulate the migration of iTregs to local tissues (30–33), and inhibitory cytokine and immune checkpoint molecule pairs such as LGALS9-SLC1A5, TGFB1-TGFBR3, PDCD1-FAM3C, and ADORA2A-NAMPT (27, 34, 35) (Fig. 5b), suggesting that the effector function of $CD8^+$ T cells can be suppressed through interactions with iTregs in the local immune microenvironment of AE patients.

DISCUSSION

The liver is an immunological organ with unique tolerogenic capacities (36). *E. multilocularis* larvae predominantly dwell in the liver and cause tumor-like AE, which elicits a severe hepatic granulomatous inflammatory response. Our previous studies have identified some larger and tolerogenic cell subsets, such as macrophages ($CD163^+$), NK cells, and T cells ($CD4^+$ and $CD8^+$) around lesions, and found that the persistence of *E. multilocularis* in the liver leads to the disruption of the normal functions of T cells and NK cells via traditional immunohistochemical and flow cytometric analyses (8, 37). Although these traditional approaches were powerful, they required prior guesswork or knowledge in order to discover various immune cell types, which introduces bias and limits the potential for discovery of new cell subsets (38, 39). scRNA-seq technology overcomes the limitations of these traditional methods, by measuring the whole transcriptome at a single-cell resolution and distinguishing different cell types and cellular states based on their transcriptional signatures, and has been widely used to explore tumor microenvironment heterogeneity (40, 41). Therefore, we used scRNA-seq technology to identify the heterogeneous composition of liver-infiltrating cells, and we generated a relatively comprehensive view of the immune atlas of the AE liver immune microenvironment with data from 4 AE patients, consisting of 83,921 single-cell profiles isolated from 4 PL tissue, 3 AN tissue, and 4 PB samples. We identified a total of 23 large clusters as well as some novel cell subsets, such as ILC2s and $CD8^+$ MAIT cells, in all the PL, AN, and PB samples with high homogeneity. The distributions and transcriptomes of these cell clusters differed between the liver and periphery and between the lesion and normal tissues, which will help us gain a deeper understanding of the heterogeneity of immune cells in the AE lesion microenvironment.

The first direct comparisons between PL or AN tissue and the PB confirmed that the immune cell subset composition was different between the liver region and peripheral immune system and that some cell clusters showed a tissue preference. In particular, the proportions of CD8_exhaustion cells, PRGDT cells, NK cells, ILCs, and pDCs were higher in the liver tissues (PL and AN), and CD8_exhaustion cells showed the highest patient consistency when comparing PL tissue with the PB. The DEGs of CD8_exhaustion cells in the PL

FIG 3 Legend (Continued)
between the PL and AN samples from the patients. MAIT cells are marked in red because there was a higher proportional change in these cells in the PL site than in the AN site. (c) Volcano plot showing the differentially expressed genes of the MAIT cells in PL and AN samples. *P* values were calculated using Student's *t* test. Genes with *P* values lower than 0.01 and the top 10 genes with the highest $\log_2$ fold changes are marked in red. Genes with *P* values lower than 0.01 and the 10 lowest $\log_2$ fold changes are marked in blue. (d) Heatmap of the significantly enriched disease terms for the genes differentially expressed in MAIT cells from PL and AN samples. GO terms related to the liver are marked in bold red text. (e) Heatmap of the significantly enriched GO terms for the genes differentially expressed in MAIT cells from PL and AN samples. GO terms related to the immune response with a smaller *P* value in the PL site than in the AN site are marked in red. GO terms related to the immune response with a smaller *P* value in the AN site than in the PL site are marked in blue. (f) Bar plot showing the counts of the top 10 TCR clones of MAIT cells in the PL site across the four AE patients. Each TCR clone was named according to its combination of VDJC genes. (g) Percentages of MAIT cells with the TCR clone TRAV1-2_TRAJ33_TRAC across PB, AN, and PL tissues for each patient.

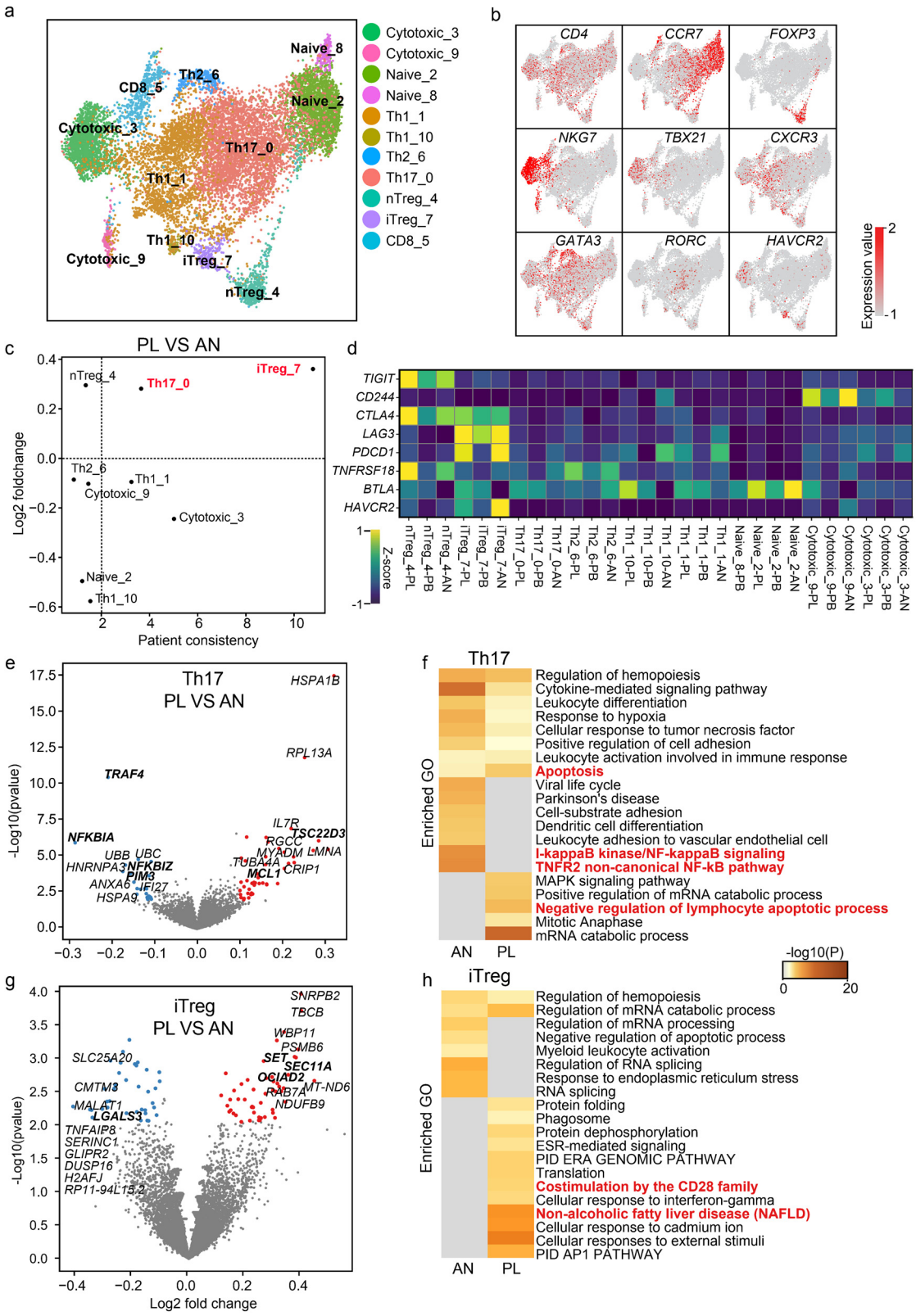

FIG 4 Th17 cells and iTregs exhibit immunosuppressive functions in PL tissue across AE patients. (a) Two-dimensional representation of CD4$^+$ T cells via UMAP; each dot represents one cell. Th1, Th1 helper cells; Th2, Th2 helper cells; Th17, Th17 helper cells; iTregs, induced regulatory T cells, nTregs, naive regulatory T cells. (b) Expression patterns of the marker genes used for cell type annotation. The expression levels of marker genes are indicated by color. (c) Differences in the proportions of cells among all cells and the consistency in differences between PL and AN samples across the patients. Th17 cells and iTregs are

(Continued on next page)

group showed enrichment of the disease term "immunosuppression," suggesting that exhausted $CD8^+$ T cells play an immunosuppressive role in the AE microenvironment that favors persistent *E. multilocularis* infection, which is consistent with our recent reports (8).

To reflect the microenvironment of metacestodes in the liver, we next compared PL tissue with the corresponding AN tissue and observed that the proportions of Mono_CD14 cells, NKT1 cells, CD4_Tregs, ILC2s, CD8_exhaustion cells, MAIT cells, pDCs, B cells, and PRGDT cells were enriched in the PL site. Notably, ILC2s showed the highest patient consistency at the PL site. ILC2s are antigen-independent innate lymphocytes that regulate inflammation and immunity to pathogens in mammalian tissues (42). Recently, ILC2s have been found to accumulate in human cancer tissues and have emerged as tissue-specific enhancers of anticancer immunity (43, 44). We found that tumor-related genes such as *IFNG*, *ANXA1*, *FOSB*, and *HSPA90AA1* were highly expressed by ILC2s in the PL site and identified enrichment of the disease terms "hepatic neoplasms" and "neoplasm metastasis," which may explain why AE lesions exhibit malignant tumor-like symptoms and the potential to metastasize to other organs. In addition, the frequency of ILC2s was reported to be increased in the fibrotic liver (45), and a main pathological feature of AE is extensive fibrosis around the lesion, indicating that ILC2s may be correlated with liver fibrosis in AE patients.

MAIT cells, as a new innate cell-like T-cell population that is clearly enriched in the human liver, constitute up to 20 to 50% of all intrahepatic T cells and may play important roles in immune homeostasis in the steady state as well as in immune defense and inflammation in liver diseases (46, 47). However, previous studies have investigated MAIT cells in infectious or autoimmune diseases and shown that the infiltration and function of this subset are substantially impaired (47, 48). In human colorectal cancer studies, activated MAIT cells accumulated in tumors were correlated with inferior patient survival (49). In human hepatocellular carcinoma (HCC), MAIT cells were found to be functionally exhausted with high expression of PD-1, CTLA4, and TIM-3 and an inability to produce IFN-γ, perforin, and granzyme B (50). In this study, we observed increased representation of $CD8^+$ MAIT cells in PL tissue compared to AN liver tissue, and these cells expressed higher levels of MYADM, FOS, LMNA, and other tumor-related genes but lower levels of cell killing- and cytokine secretion-related genes, such as GZMA and CXCR6, in PL tissue, indicating that the function of $CD8^+$ MAIT cells was also impaired in PL tissue, consistent with previous studies in HCC. Furthermore, the DEGs highly expressed in PL tissue were enriched in the terms "neoplastic cell transformation" and "lung neoplasms and carcinoma." GO term enrichment analysis of the DEGs highly expressed in PL tissue showed enrichment in the negative regulation of cytokine production, apoptotic signaling pathway, positive regulation of cell migration, and regulation of extracellular matrix assembly. These results indicate that MAIT cells in the AE tissue microenvironment have functions related to suppressing the immune response and promoting apoptosis and cell migration, which further explains why AE patients exhibit severe pathological damage to the liver and growth with a malignant tumor-like pattern. Therefore, strategies to modulate the functional activities of $CD8^+$ MAIT cells from exhausted to effector-like cells might be a possible immunotherapy for AE. Notably, TCR-seq results showed that the TRAV1-2_TRAJ33_TRAC TCR exhibited significant clonal expansion in MAIT cells from all patients, indicating that

FIG 4 Legend (Continued)
marked in red because there were higher proportional changes in these cells in the PL site than in the AN site. (d) Expression patterns of exhaustion-related molecules in $CD4^+$ T cells across PB, AN, and PL samples. The means of the expression levels of the marker genes are indicated by color. (e) Volcano plot showing the differentially expressed genes of Th17 cells in PL and AN samples. *P* values were calculated using Student's *t* test. Genes with a *P* value lower than 0.01 and $\log_2$ fold change higher than 0.1 are marked in red. Genes with a *P* value lower than 0.01 and $\log_2$ fold change lower than -0.1 are marked in blue. (f) Heatmap of the significantly enriched GO terms for the genes differentially expressed in Th17 cells from PL and AN samples. GO terms related to the immune response are marked in bold red text. MAPK, mitogen-activated protein kinase. (g) Volcano plot showing the differentially expressed genes of iTregs in PL and AN samples. *P* values were calculated using Student's *t* test. Genes with a *P* value lower than 0.01 and $\log_2$ fold change higher than 0.1 are marked in red. Genes with a *P* value lower than 0.01 and $\log_2$ fold change lower than -0.1 are marked in blue. (h) Heatmap of the significantly enriched GO terms for the genes differentially expressed in iTregs from PL and AN samples. GO terms related to the immune response are marked in bold red text. ESR, erythrocyte sedimentation rate.

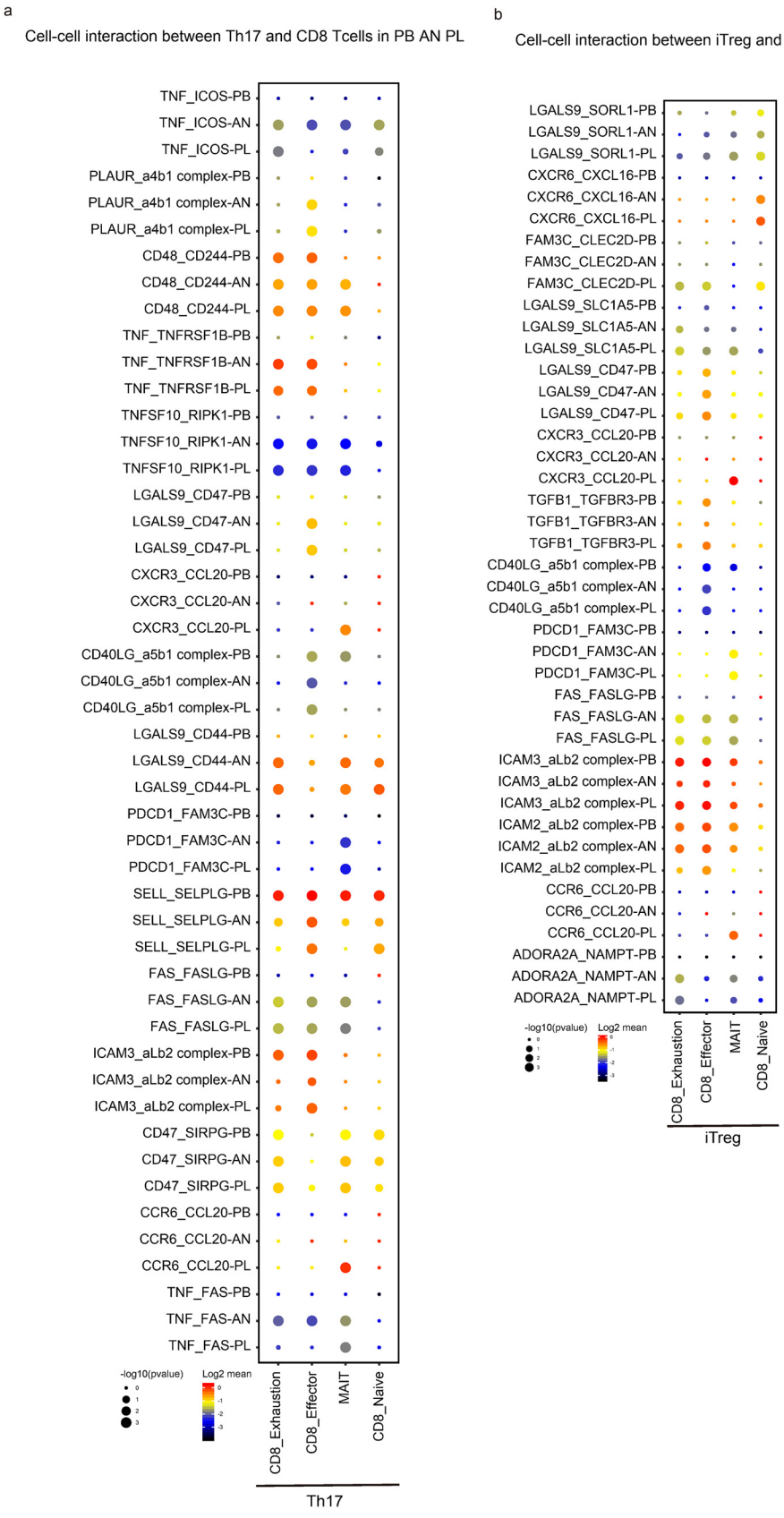

FIG 5 Interactions of iTregs and Th17 cells with CD8$^+$ T cells in the AE lesion microenvironment. (a) Dot plot of the interactions between Th17 and CD8$^+$ T cells in PL, AN, and PB tissues predicted by CellPhoneDB. Each row in the cell-cell

(Continued on next page)

this TCR may respond to parasite antigens and that vaccines based on this receptor may prevent the occurrence of AE in patients.

$CD4^+$ T lymphocytes, the major cell population involved in the cell-mediated immune response, have been reported to play a crucial role in mounting a granulomatous inflammatory response and achieving resistance to *E. multilocularis* infection; these cells are highly associated with abortive or chronic parasitism by the metacestode in AE patients (7). Depending on the changes in different cytokine-induced microenvironments, $CD4^+$ T lymphocytes can differentiate into different subsets and perform different functions (51, 52). Here, we reclustered all $CD4^+$ T cells and obtained a total of 11 subclusters, and we found that the proportions of iTregs, nTregs, and Th17 cells were significantly increased in the PL site compared to the AN site and that iTregs and Th17 cells showed high patient consistency, which is consistent with previous studies showing that Tregs gradually accumulate during the course of both chronic human AE and murine AE (9, 53). DEG expression analysis of iTregs in PL and AN tissues showed that oncogenes (*SET*, *OCIAD2*, and *SEC11A*) were highly expressed in the PL site, which promoted cell invasion and tumor metastasis. DEG analysis of Th17 cells in PL and AN tissues showed that genes related to the inhibition of inflammation and the immune response were highly expressed in the PL site and enriched in apoptosis-related GO terms, further indicating that the AE tissue microenvironment was in a state of immunosuppression. In addition, recent studies have shown that the expression of coinhibitory molecules by Tregs is critical for Treg differentiation and function. For example, Tregs expressing TIGIT selectively inhibit proinflammatory Th1- and Th17-cell responses but not Th2-cell responses (54). We further analyzed the expression of coinhibitory molecules in $CD4^+$ T cells from PB, AN, and PL samples and found that Tregs had higher expression of most of the coinhibitory molecules (TIGIT, *PDCD1*, *CTLA4*, *LAG3*, and *HAVCR2*) than other $CD4^+$ T cells, and previous work reported that depletion of $FoxP3^+$ Tregs in experimental animals resulted in a significantly lower parasite load by promoting costimulation and Th1/17 immune responses (55). We speculated that the preferential accumulation of Tregs in PL tissue may inhibit proinflammatory Th1- and Th17-cell responses in AE, favoring metacestode survival, which is regulated by the expression of coinhibitory molecules.

With the development of scRNA-seq technology, a range of analysis tools is gradually developing and improving, which allowed us to identify the potential cellular communication in the liver immune microenvironment. The CellPhoneDB analysis tool was recently used to predict the interactions between different cell types based on their ligand and corresponding receptor expression. If the *P* value of a ligand-receptor pair between two cell types is lower than 0.05, the ligand-receptor pair is considered an interaction pair between two cell types. It has been successfully used to predict the interactions between tissue-resident Th17 cells and myeloid cells in the lungs of severe COVID-19 patients (56), and these predictions were reliable and can be verified experimentally (56, 57). In this study, we found a close contact between $CD8^+$ T cells and iTregs or Th17 cells by this tool, especially based on genes related to immunosuppression, such as the PDCD1-FAM3C pair that was highly expressed in PL tissue, suggesting that cellular interactions result in an inhibitory microenvironment in AE lesions.

Overall, we used scRNA-seq to elucidate the global landscape of single $CD45^+$ lymphocytes in different tissues from four hepatic AE patients and revealed detailed char-

FIG 5 Legend (Continued)
interaction plot represents a ligand-receptor interaction pair. The ligand-receptor interaction pairs with higher expression in PL and AN samples than in PB samples were selected. The first interaction partner was considered to be expressed on Th17 cells, and the second interaction partner was considered to be expressed on the $CD8^+$ T-cell subtypes. *P* values are indicated by the size of the circle, as shown in the scale below (permutation test). The means of the average expression levels of interacting molecule 1 in cluster 1 and interacting molecule 2 in cluster 2 are indicated by color. (b) Dot plot of the interactions between iTregs and $CD8^+$ T cells in PL, AN, and PB tissues predicted by CellPhoneDB. Each row in the cell-cell interaction plot represents a ligand-receptor interaction pair. The ligand-receptor interaction pairs with higher expression in PL and AN samples than in PB samples were selected. The first interaction partner was considered to be expressed on iTregs, and the second interaction partner was considered to be expressed on the $CD8^+$ T-cell subtypes. *P* values are indicated by the size of the circle, as shown in the scale below (permutation test). The means of the average expression levels of interacting molecule 1 in cluster 1 and interacting molecule 2 in cluster 2 are indicated by color.

acteristics of the AE liver and peripheral microenvironments in terms of cell clustering, differential expression analysis, and unique signatures. This study uncovers some important novel lymphocytes in the AE liver microenvironment. Higher levels of ILC2s and impaired $CD8^+$ MAIT cell and iTreg infiltration in PL liver tissues blunting immune responses may play critical roles in building an "immunosuppressive microenvironment" for AE and favoring metacestode survival. These observations will pave the way toward both a deeper understanding of AE pathogenesis and immune cell heterogeneity in the AE lesion microenvironment and the development of more effective personalized therapeutic approaches for AE.

MATERIALS AND METHODS

Ethics statement. The design of this study was in accordance with the Helsinki Declaration (58). All samples were obtained after written and signed informed consent was obtained from all patients or their legal representatives, and the study was approved by the Human Ethics Committee of First Affiliated Hospital of Xinjiang Medical University. Patients under the age of 18 were not included in this study.

Human subjects and specimen collection. Four AE patients who were pathologically and radiographically (computed tomography [CT] and magnetic resonance imaging [MRI]) diagnosed were enrolled in this study. Three of these patients were female, and one was male. Their ages ranged from 22 to 60 years, with a median age of 42 years. None of the patients received drug or surgical treatment prior to lesion resection, with the exception of P12, who was treated with albendazole (ABZ) for 4 months. Patients with hepatitis B virus (HBV), hepatitis C virus (HCV), or human immunodeficiency virus (HIV) infection or other immunodeficiency conditions were excluded to eliminate other confounding infectious and autoimmune disorders. The basic clinical characteristics of the patients are summarized in Table S1 in the supplemental material. PB samples were obtained from the patients before surgery, and liver tissue samples were collected from each patient during surgical resection. For patients P03, P12, and P13, their PB and paired fresh PL (approximately 0.5 cm from a lesion) and AN (at least 2 cm distant from the lesion) liver tissues, as described in the work of Zhang et al. (8), were obtained for subsequent pathological examination and lymphocyte isolation. For patient P03, only fresh PL liver tissues and matched PB were collected. The study protocol was approved by the Ethics Committee of the First Affiliated Hospital of Xinjiang Medical University. All patients in this study provided written informed consent for sample collection and data analysis.

Single-cell preparation. Lymphocytes were isolated from human PB and liver tissue samples according to the protocol described in a previous report (15). Briefly, peripheral blood mononuclear cells (PBMCs) were isolated using Ficoll (Solarbio, Beijing, China) density gradient centrifugation, and 3 mL of fresh PB was collected in EDTA anticoagulant-treated tubes, subsequently diluted with 3 mL of phosphate-buffered saline (PBS; Solarbio), and then carefully added to the top of 3 mL of Ficoll solution. After centrifugation at 400 $\times$ *g* and 25°C for 30 min, the PBMCs were carefully transferred to a new tube, washed twice with PBS at 1,500 rpm and 4°C for 5 min, and resuspended in sorting buffer (PBS supplemented with 1% fetal bovine serum [FBS; HyClone, Boston, MA, USA]). For isolation of mononuclear cells from liver tissues, fresh PL and AN liver tissues from AE patients were cut into small pieces, followed by digestion with collagenase IV (Sigma, St. Louis, MO, USA) and DNase I (Roche, Basel, Switzerland) in RPMI 1640 medium at 37°C for 30 min. The digested tissues were then filtered through 100-μm mesh and separated by centrifugation with Ficoll (Solarbio), and the pelleted cells were suspended in red blood cell lysis buffer (Solarbio) to remove the red blood cells. After being washed twice with 1$\times$ PBS, the cell pellets were resuspended in sorting buffer.

Then, the single-cell suspensions of lymphocytes derived from the human PB, PL, and AN liver tissue samples were blocked with mouse serum for 20 min at 4°C and then stained with an anti-CD45 antibody (BioLegend, San Diego, CA, USA) for 30 min at 4°C. $CD45^+$ cells were sorted using an LSRFortessa flow cytometer (BD Immunocytometry Systems, San Diego, CA) and collected for further scRNA-seq analysis.

Single-cell RNA sequencing. (i) Cell capture and cDNA synthesis. Using the single-cell 5′ library and gel bead kit (10X Genomics, catalog no. 1000006) and Chromium single-cell A chip kit (10X Genomics, catalog no. 120236), a cell suspension (300 to 600 living cells per microliter determined by Count Star) was loaded onto the Chromium single-cell controller (10X Genomics) to generate single-cell gel beads-in-emulsion according to the manufacturer's protocol. In short, single cells were suspended in PBS containing 0.04% bovine serum albumin (BSA). Approximately 6,000 cells were added to each channel, and the number of target cells recovered was estimated to be approximately 3,000. The captured cells were lysed, and the released RNA was barcoded through reverse transcription in individual gel beads-in-emulsion. Reverse transcription was performed on an S1000 Touch thermal cycler (Bio-Rad) at 53°C for 45 min followed by 85°C for 5 min. The corresponding cDNA was generated and then amplified, and quality was assessed using an Agilent 4200 (performed by CapitalBio, Beijing, China).

(ii) scRNA-seq library preparation. According to the manufacturer's instructions, scRNA-seq libraries were constructed using the single-cell 5′ library and gel bead kit. The libraries were sequenced on an Illumina Novaseq6000 sequencer with a sequencing depth of at least 100,000 reads per cell using the paired-end 150-bp (PE150) reading strategy (performed by CapitalBio, Beijing, China).

Data preprocessing. (i) scRNA-seq data processing. scRNA-seq reads were aligned with the GRCh37 (hg19) reference genome and quantified using cellranger count (10X Genomics, v.2.0.0). To filter out cells whose transcripts were captured at low levels, we first plotted the distribution of genes

detected and nFeature_RNA for all experiments. On the basis of these plots, we chose to filter out cells that had fewer than 1,000 nFeature_RNAs. For all expression matrices, the expression value of each gene in each cell was normalized by the following conversions: total read counts of the cell multiplied by 10,000 and then log-transformed (natural logarithm, ln [value + 1]).

(ii) Single-cell TCR sequencing (scTCR-seq) data processing. scRNA-seq reads were aligned with the refdata-cellranger-vdj-GRCh37-alts-ensembl-2.0.0 reference genome and quantified using cellranger vdj (10X Genomics, v.2.0.0). Then, the number of reads for each TCR in each cell was counted.

(iii) scRNA-seq data integration and clustering. Using the Seurat v3 (17) package, variable genes were detected in each matrix and used as the input for the 'FindIntegrationAnchors' function; thus, six matrices were integrated with the 'IntegrateData' function. The integrated data were then clustered with principal-component analysis (PCA; the top 50 principal components were used for all data), and the clusters were visualized in two dimensions with uniform manifold approximation and projection (UMAP). All data alignment, integration, and clustering were performed under the standard Seurat workflow.

(iv) Cell type proportion analysis with scRNA-seq data. The proportion of each cell type in every patient was calculated using the 'prop.table' and 'table' R functions. In every patient, the sum of the proportions of all cell types was set equal to 1. The $\log_2$ fold changes in every cell type proportion for PL versus AN, AN versus PB, and PL versus PB for each patient were calculated by taking the base 2 logarithm of the quotient of the two proportions.

(v) Differential expression analysis. To identify differentially expressed genes (DEGs), we used a *t* test to search for the DEGs between each pair of cells obtained from the three groups (i.e., the PB, AN, and PL groups). We applied multiple thresholds to screen DEGs, including a mean log fold change of >0.2 and a *P* value of <0.01. We then compared these DEG groups to the Metascape (59) website (https://metascape.org/gp/index.html#/main/step1) and used the default parameters to perform gene ontology (GO) analysis for each stage.

(vi) Cytokine-cytokine receptor interaction analysis. To identify potential cellular communication between $CD8^+$ T cells and other $CD4^+$ T-cell types (Th17 cells and induced Tregs [iTregs]), we applied the CellPhoneDB algorithm (23) to the scRNA-seq profiles of the PB, AN, and PL samples of the four hepatic AE patients. CellPhoneDB evaluated the impact of the ligand-receptor interactions based on the ligand expression in one cell type and corresponding receptor expression in another cell type. If a *P* value of a ligand-receptor pair between two cell types is lower than 0.05, the ligand-receptor pair is considered an interaction pair between two cell types. We focused on the enriched cytokine-receptor interactions between Th17 cells and $CD8^+$ T cells and between iTregs and $CD8^+$ T cells and selected the cytokine-receptor interactions associated with highly significant ($P < 0.01$) cell-cell interaction pairs.

Data availability. The raw sequencing data have been deposited in the Genome Sequence Archive (60) in the BIG Data Center (61), Beijing Institute of Genomics (BIG), Chinese Academy of Sciences, under accession number HRA000553; they are publicly accessible at https://bigd.big.ac.cn/gsa-human/browse/HRA000553. The processed data are provided on figshare (https://figshare.com/s/f2a4578be27c2cb767f9). All the other data generated in this study are included in the article and supplemental material.

SUPPLEMENTAL MATERIAL

Supplemental material is available online only.

SUPPLEMENTAL FILE 1, PDF file, 9.3 MB.

ACKNOWLEDGMENTS

We thank Zhigang Tian (University of Science and Technology of China). We also thank the USTC supercomputing center and the School of Life Science Bioinformatics Center for providing supercomputing resources for this project.

This work was supported by the Xinjiang Uyghur Autonomous Region Key Laboratory Open Research Project (2019D04021), the Special Funds for Development of Local Science and Technology from Central Government (ZYYD2022B06), and the State Key Laboratory of Pathogenesis, Prevention and Treatment of Central Asia High Incidence Diseases Fund (SKL-HIDCA-2022-BC1).

T. Jiang, W. Sun, K. Qu, C. Zhang, and H. Wang designed the study. T. Aji, J. Hou, and A. Yasen performed the tissue sampling. W. Sun and C. Guo analyzed the scRNA-seq data. T. Aji, Y. Shao, B. Ran, and Q. Guo provided the human samples. T. Jiang, W. Sun, and H. Wang drafted the manuscript. K. Qu and H. Wen critically revised the manuscript. All authors read and approved the final manuscript.

We declare that we have no competing interests.

REFERENCES

1. Wen H, Vuitton L, Tuxun T, Li J, Vuitton DA, Zhang W, McManus DP. 2019. Echinococcosis: advances in the 21st century. Clin Microbiol Rev 32:e00075-18. https://doi.org/10.1128/CMR.00075-18.
2. Baumann S, Shi R, Liu W, Bao H, Schmidberger J, Kratzer W, Li W, Interdisciplinary Echinococcosis Working Group Ulm. 2019. Worldwide literature on epidemiology of human alveolar echinococcosis: a systematic review

of research published in the twenty-first century. Infection 47:703–727. https://doi.org/10.1007/s15010-019-01325-2.
3. Torgerson PR, Keller K, Magnotta M, Ragland N. 2010. The global burden of alveolar echinococcosis. PLoS Negl Trop Dis 4:e722. https://doi.org/10.1371/journal.pntd.0000722.
4. Reinehr M, Micheloud C, Grimm F, Kronenberg PA, Grimm J, Beck A, Nell J, Meyer Zu Schwabedissen C, Furrer E, Mullhaupt B, Barth TFE, Deplazes P, Weber A. 2020. Pathology of echinococcosis: a morphologic and immunohistochemical study on 138 specimens with focus on the differential diagnosis between cystic and alveolar echinococcosis. Am J Surg Pathol 44:43–54. https://doi.org/10.1097/PAS.0000000000001374.
5. Torgerson PR, Schweiger A, Deplazes P, Pohar M, Reichen J, Ammann RW, Tarr PE, Halkic N, Mullhaupt B. 2008. Alveolar echinococcosis: from a deadly disease to a well-controlled infection. Relative survival and economic analysis in Switzerland over the last 35 years. J Hepatol 49:72–77. https://doi.org/10.1016/j.jhep.2008.03.023.
6. Chauchet A, Grenouillet F, Knapp J, Richou C, Delabrousse E, Dentan C, Millon L, Di Martino V, Contreras R, Deconinck E, Blagosklonov O, Vuitton DA, Bresson-Hadni S, FrancEchino Network. 2014. Increased incidence and characteristics of alveolar echinococcosis in patients with immunosuppression-associated conditions. Clin Infect Dis 59:1095–1104. https://doi.org/10.1093/cid/ciu520.
7. Gottstein B, Soboslay P, Ortona E, Wang J, Siracusano A, Vuitton D. 2017. Immunology of alveolar and cystic echinococcosis (AE and CE). Adv Parasitol 96:1–54. https://doi.org/10.1016/bs.apar.2016.09.005.
8. Zhang C, Lin R, Li Z, Yang S, Bi X, Wang H, Aini A, Zhang N, Abulizi A, Sun C, Li L, Zhao Z, Qin R, Li X, Li L, Aji T, Shao Y, Vuitton DA, Tian Z, Wen H. 2020. Immune exhaustion of T cells in alveolar echinococcosis patients and its reversal by blocking checkpoint receptor TIGIT in a murine model. Hepatology 71:1297–1315. https://doi.org/10.1002/hep.30896.
9. Zhang C, Shao Y, Yang S, Bi X, Li L, Wang H, Yang N, Li Z, Sun C, Li L, Lu G, Aji T, Vuitton DA, Lin R, Wen H. 2017. T-cell tolerance and exhaustion in the clearance of Echinococcus multilocularis: role of inoculum size in a quantitative hepatic experimental model. Sci Rep 7:11153. https://doi.org/10.1038/s41598-017-11703-1.
10. Hubner MP, Manfras BJ, Margos MC, Eiffler D, Hoffmann WH, Schulz-Key H, Kern P, Soboslay PT. 2006. Echinococcus multilocularis metacestodes modulate cellular cytokine and chemokine release by peripheral blood mononuclear cells in alveolar echinococcosis patients. Clin Exp Immunol 145:243–251. https://doi.org/10.1111/j.1365-2249.2006.03142.x.
11. Wang J, Cardoso R, Marreros N, Muller N, Lundstrom-Stadelmann B, Siffert M, Vuitton DA, Boue F, Lin R, Wen H, Gottstein B. 2018. Foxp3(+) T regulatory cells as a potential target for immunotherapy against primary infection with *Echinococcus multilocularis* eggs. Infect Immun 86:e00542-18. https://doi.org/10.1128/IAI.00542-18.
12. Luecken MD, Theis FJ. 2019. Current best practices in single-cell RNA-seq analysis: a tutorial. Mol Syst Biol 15:e8746. https://doi.org/10.15252/msb.20188746.
13. Zheng C, Zheng L, Yoo JK, Guo H, Zhang Y, Guo X, Kang B, Hu R, Huang JY, Zhang Q, Liu Z, Dong M, Hu X, Ouyang W, Peng J, Zhang Z. 2017. Landscape of infiltrating T cells in liver cancer revealed by single-cell sequencing. Cell 169:1342–1356.e16. https://doi.org/10.1016/j.cell.2017.05.035.
14. Tirosh I, Izar B, Prakadan SM, Wadsworth MH, II, Treacy D, Trombetta JJ, Rotem A, Rodman C, Lian C, Murphy G, Fallahi-Sichani M, Dutton-Regester K, Lin JR, Cohen O, Shah P, Lu D, Genshaft AS, Hughes TK, Ziegler CG, Kazer SW, Gaillard A, Kolb KE, Villani AC, Johannessen CM, Andreev AY, Van Allen EM, Bertagnolli M, Sorger PK, Sullivan RJ, Flaherty KT, Frederick DT, Jane-Valbuena J, Yoon CH, Rozenblatt-Rosen O, Shalek AK, Regev A, Garraway LA. 2016. Dissecting the multicellular ecosystem of metastatic melanoma by single-cell RNA-seq. Science 352:189–196. https://doi.org/10.1126/science.aad0501.
15. Yasen A, Sun W, Aini A, Aji T, Shao Y, Wang H, Li K, Li W, Zhang C, Ahan A, Jiang T, Wang Z, Zhang W, Sun C, Qu K, Wen H. 2021. Single-cell RNA sequencing reveals the heterogeneity of infiltrating immune cell profiles in the hepatic cystic echinococcosis microenvironment. Infect Immun 89:e0029721. https://doi.org/10.1128/IAI.00297-21.
16. Han A, Glanville J, Hansmann L, Davis MM. 2014. Linking T-cell receptor sequence to functional phenotype at the single-cell level. Nat Biotechnol 32:684–692. https://doi.org/10.1038/nbt.2938.
17. Stuart T, Butler A, Hoffman P, Hafemeister C, Papalexi E, Mauck WM, III, Hao Y, Stoeckius M, Smibert P, Satija R. 2019. Comprehensive integration of single-cell data. Cell 177:1888–1902.e21. https://doi.org/10.1016/j.cell.2019.05.031.
18. Collier JL, Weiss SA, Pauken KE, Sen DR, Sharpe AH. 2021. Not-so-opposite ends of the spectrum: CD8(+) T cell dysfunction across chronic infection, cancer and autoimmunity. Nat Immunol 22:809–819. https://doi.org/10.1038/s41590-021-00949-7.
19. Zhang N, Bevan MJ. 2011. CD8(+) T cells: foot soldiers of the immune system. Immunity 35:161–168. https://doi.org/10.1016/j.immuni.2011.07.010.
20. Taniguchi K, Karin M. 2018. NF-kappaB, inflammation, immunity and cancer: coming of age. Nat Rev Immunol 18:309–324. https://doi.org/10.1038/nri.2017.142.
21. Oue N, Naito Y, Hayashi T, Takigahira M, Kawano-Nagatsuma A, Sentani K, Sakamoto N, Zarni Oo H, Uraoka N, Yanagihara K, Ochiai A, Sasaki H, Yasui W. 2014. Signal peptidase complex 18, encoded by SEC11A, contributes to progression via TGF-alpha secretion in gastric cancer. Oncogene 33:3918–3926. https://doi.org/10.1038/onc.2013.364.
22. Feeley EM, Pilla-Moffett DM, Zwack EE, Piro AS, Finethy R, Kolb JP, Martinez J, Brodsky IE, Coers J. 2017. Galectin-3 directs antimicrobial guanylate binding proteins to vacuoles furnished with bacterial secretion systems. Proc Natl Acad Sci U S A 114:E1698–E1706. https://doi.org/10.1073/pnas.1615771114.
23. Efremova M, Vento-Tormo M, Teichmann SA, Vento-Tormo R. 2020. CellPhoneDB: inferring cell-cell communication from combined expression of multi-subunit ligand-receptor complexes. Nat Protoc 15:1484–1506. https://doi.org/10.1038/s41596-020-0292-x.
24. Dehmani S, Nerriere-Daguin V, Neel M, Elain-Duret N, Heslan JM, Belarif L, Mary C, Thepenier V, Biteau K, Poirier N, Blancho G, Haspot F. 2021. SIRP-gamma-CD47 interaction positively regulates the activation of human T cells in situation of chronic stimulation. Front Immunol 12:732530. https://doi.org/10.3389/fimmu.2021.732530.
25. Agresta L, Hoebe KHN, Janssen EM. 2018. The emerging role of CD244 signaling in immune cells of the tumor microenvironment. Front Immunol 9:2809. https://doi.org/10.3389/fimmu.2018.02809.
26. Oo YH, Banz V, Kavanagh D, Liaskou E, Withers DR, Humphreys E, Reynolds GM, Lee-Turner L, Kalia N, Hubscher SG, Klenerman P, Eksteen B, Adams DH. 2012. CXCR3-dependent recruitment and CCR6-mediated positioning of Th-17 cells in the inflamed liver. J Hepatol 57:1044–1051. https://doi.org/10.1016/j.jhep.2012.07.008.
27. Yang RY, Sun LL, Li CF, Wang YH, Yao J, Li H, Yan MS, Chang WC, Hsu JM, Cha JH, Hsu JL, Chou CW, Sun X, Deng YL, Chou CK, Yu DH, Hung MC. 2021. Galectin-9 interacts with PD-1 and TIM-3 to regulate T cell death and is a target for cancer immunotherapy. Nat Commun 12:832. https://doi.org/10.1038/s41467-021-21099-2.
28. Strasser A, Jost PJ, Nagata S. 2009. The many roles of FAS receptor signaling in the immune system. Immunity 30:180–192. https://doi.org/10.1016/j.immuni.2009.01.001.
29. Elgueta R, Benson MJ, de Vries VC, Wasiuk A, Guo Y, Noelle RJ. 2009. Molecular mechanism and function of CD40/CD40L engagement in the immune system. Immunol Rev 229:152–172. https://doi.org/10.1111/j.1600-065X.2009.00782.x.
30. Chen D, Bromberg JS. 2006. T regulatory cells and migration. Am J Transplant 6:1518–1523. https://doi.org/10.1111/j.1600-6143.2006.01372.x.
31. Koch MA, Tucker-Heard G, Perdue NR, Killebrew JR, Urdahl KB, Campbell DJ. 2009. The transcription factor T-bet controls regulatory T cell homeostasis and function during type 1 inflammation. Nat Immunol 10:595–602. https://doi.org/10.1038/ni.1731.
32. Littringer K, Moresi C, Rakebrandt N, Zhou XB, Schorer M, Dolowschiak T, Kirchner F, Rost F, Keller CW, McHugh D, LeibundGut-Landmann S, Robinson MD, Joller N. 2018. Common features of regulatory T cell specialization during Th1 responses. Front Immunol 9:1344. https://doi.org/10.3389/fimmu.2018.01344.
33. Yamazaki T, Yang XO, Chung Y, Fukunaga A, Nurieva R, Pappu B, Martin-Orozco N, Kang HS, Ma L, Panopoulos AD, Craig S, Watowich SS, Jetten AM, Tian Q, Dong C. 2008. CCR6 regulates the migration of inflammatory and regulatory T cells. J Immunol 181:8391–8401. https://doi.org/10.4049/jimmunol.181.12.8391.
34. Derynck R, Turley SJ, Akhurst RJ. 2021. TGFbeta biology in cancer progression and immunotherapy. Nat Rev Clin Oncol 18:9–34. https://doi.org/10.1038/s41571-020-0403-1.
35. Ma SR, Deng WW, Liu JF, Mao L, Yu GT, Bu LL, Kulkarni AB, Zhang WF, Sun ZJ. 2017. Blockade of adenosine A2A receptor enhances CD8(+) T cells response and decreases regulatory T cells in head and neck squamous cell carcinoma. Mol Cancer 16:99. https://doi.org/10.1186/s12943-017-0665-0.
36. Heymann F, Tacke F. 2016. Immunology in the liver–from homeostasis to disease. Nat Rev Gastroenterol Hepatol 13:88–110. https://doi.org/10.1038/nrgastro.2015.200.

37. Wang H, Zhang CS, Fang BB, Hou J, Li WD, Li ZD, Li L, Bi XJ, Li L, Abulizi A, Shao YM, Lin RY, Wen H. 2020. Dual role of hepatic macrophages in the establishment of the Echinococcus multilocularis metacestode in mice. Front Immunol 11:600635. https://doi.org/10.3389/fimmu.2020.600635.
38. Spitzer MH, Nolan GP. 2016. Mass cytometry: single cells, many features. Cell 165:780–791. https://doi.org/10.1016/j.cell.2016.04.019.
39. Perfetto SP, Chattopadhyay PK, Roederer M. 2004. Seventeen-colour flow cytometry: unravelling the immune system. Nat Rev Immunol 4:648–655. https://doi.org/10.1038/nri1416.
40. Zhang Y, Wang D, Peng M, Tang L, Ouyang J, Xiong F, Guo C, Tang Y, Zhou Y, Liao Q, Wu X, Wang H, Yu J, Li Y, Li X, Li G, Zeng Z, Tan Y, Xiong W. 2021. Single-cell RNA sequencing in cancer research. J Exp Clin Cancer Res 40:81. https://doi.org/10.1186/s13046-021-01874-1.
41. Papalexi E, Satija R. 2018. Single-cell RNA sequencing to explore immune cell heterogeneity. Nat Rev Immunol 18:35–45. https://doi.org/10.1038/nri.2017.76.
42. Vivier E, van de Pavert SA, Cooper MD, Belz GT. 2016. The evolution of innate lymphoid cells. Nat Immunol 17:790–794. https://doi.org/10.1038/ni.3459.
43. Moral JA, Leung J, Rojas LA, Ruan J, Zhao J, Sethna Z, Ramnarain A, Gasmi B, Gururajan M, Redmond D, Askan G, Bhanot U, Elyada E, Park Y, Tuveson DA, Gonen M, Leach SD, Wolchok JD, DeMatteo RP, Merghoub T, Balachandran VP. 2020. ILC2s amplify PD-1 blockade by activating tissue-specific cancer immunity. Nature 579:130–135. https://doi.org/10.1038/s41586-020-2015-4.
44. Salimi M, Wang R, Yao X, Li X, Wang X, Hu Y, Chang X, Fan P, Dong T, Ogg G. 2018. Activated innate lymphoid cell populations accumulate in human tumour tissues. BMC Cancer 18:341. https://doi.org/10.1186/s12885-018-4262-4.
45. Forkel M, Berglin L, Kekalainen E, Carlsson A, Svedin E, Michaelsson J, Nagasawa M, Erjefalt JS, Mori M, Flodstrom-Tullberg M, Bergquist A, Ljunggren HG, Westgren M, Lindforss U, Friberg D, Jorns C, Ellis E, Bjorkstrom NK, Mjosberg J. 2017. Composition and functionality of the intrahepatic innate lymphoid cell-compartment in human nonfibrotic and fibrotic livers. Eur J Immunol 47:1280–1294. https://doi.org/10.1002/eji.201646890.
46. Provine NM, Klenerman P. 2020. MAIT cells in health and disease. Annu Rev Immunol 38:203–228. https://doi.org/10.1146/annurev-immunol-080719-015428.
47. Chen Y, Tian Z. 2021. Innate lymphocytes: pathogenesis and therapeutic targets of liver diseases and cancer. Cell Mol Immunol 18:57–72. https://doi.org/10.1038/s41423-020-00561-z.
48. Chen Y, Tian Z. 2020. Roles of hepatic innate and innate-like lymphocytes in nonalcoholic steatohepatitis. Front Immunol 11:1500. https://doi.org/10.3389/fimmu.2020.01500.
49. Zabijak L, Attencourt C, Guignant C, Chatelain D, Marcelo P, Marolleau JP, Treiner E. 2015. Increased tumor infiltration by mucosal-associated invariant T cells correlates with poor survival in colorectal cancer patients. Cancer Immunol Immunother 64:1601–1608. https://doi.org/10.1007/s00262-015-1764-7.
50. Duan M, Goswami S, Shi JY, Wu LJ, Wang XY, Ma JQ, Zhang Z, Shi Y, Ma LJ, Zhang S, Xi RB, Cao Y, Zhou J, Fan J, Zhang XM, Gao Q. 2019. Activated and exhausted MAIT cells foster disease progression and indicate poor outcome in hepatocellular carcinoma. Clin Cancer Res 25:3304–3316. https://doi.org/10.1158/1078-0432.CCR-18-3040.
51. Jiang L, Tang C, Gong Y, Liu Y, Rao J, Chen S, Qu W, Wu D, Lei L, Chen L. 2018. PD-1/PD-L1 regulates Treg differentiation in pregnancy-induced hypertension. Braz J Med Biol Res 51:e7334. https://doi.org/10.1590/1414-431x20187334.
52. Ribeiro VR, Romao-Veiga M, Romagnoli GG, Matias ML, Nunes PR, Borges VTM, Peracoli JC, Peracoli MTS. 2017. Association between cytokine profile and transcription factors produced by T-cell subsets in early- and late-onset pre-eclampsia. Immunology 152:163–173. https://doi.org/10.1111/imm.12757.
53. Nono JK, Lutz MB, Brehm K. 2014. EmTIP, a T-cell immunomodulatory protein secreted by the tapeworm Echinococcus multilocularis is important for early metacestode development. PLoS Negl Trop Dis 8:e2632. https://doi.org/10.1371/journal.pntd.0002632.
54. Joller N, Lozano E, Burkett PR, Patel B, Xiao S, Zhu C, Xia J, Tan TG, Sefik E, Yajnik V, Sharpe AH, Quintana FJ, Mathis D, Benoist C, Hafler DA, Kuchroo VK. 2014. Treg cells expressing the coinhibitory molecule TIGIT selectively inhibit proinflammatory Th1 and Th17 cell responses. Immunity 40:569–581. https://doi.org/10.1016/j.immuni.2014.02.012.
55. Wang J, Muller S, Lin R, Siffert M, Vuitton DA, Wen H, Gottstein B. 2017. Depletion of FoxP3(+) Tregs improves control of larval Echinococcus multilocularis infection by promoting co-stimulation and Th1/17 immunity. Immun Inflamm Dis 5:435–447. https://doi.org/10.1002/iid3.181.
56. Zhao Y, Kilian C, Turner JE, Bosurgi L, Roedl K, Bartsch P, Gnirck AC, Cortesi F, Schultheiss C, Hellmig M, Enk LUB, Hausmann F, Borchers A, Wong MN, Paust HJ, Siracusa F, Scheibel N, Herrmann M, Rosati E, Bacher P, Kylies D, Jarczak D, Lutgehetmann M, Pfefferle S, Steurer S, Zur-Wiesch JS, Puelles VG, Sperhake JP, Addo MM, Lohse AW, Binder M, Huber S, Huber TB, Kluge S, Bonn S, Panzer U, Gagliani N, Krebs CF. 2021. Clonal expansion and activation of tissue-resident memory-like Th17 cells expressing GM-CSF in the lungs of severe COVID-19 patients. Sci Immunol 6:eabf6692. https://doi.org/10.1126/sciimmunol.abf6692.
57. Mogilenko DA, Shpynov O, Andhey PS, Arthur L, Swain A, Esaulova E, Brioschi S, Shchukina I, Kerndl M, Bambouskova M, Yao Z, Laha A, Zaitsev K, Burdess S, Gillfilan S, Stewart SA, Colonna M, Artyomov MN. 2021. Comprehensive profiling of an aging immune system reveals clonal GZMK(+) CD8(+) T cells as conserved hallmark of inflammaging. Immunity 54:99–115.e12. https://doi.org/10.1016/j.immuni.2020.11.005.
58. World Medical Association. 2013. World Medical Association Declaration of Helsinki: ethical principles for medical research involving human subjects. JAMA 310:2191–2194. https://doi.org/10.1001/jama.2013.281053.
59. Zhou Y, Zhou B, Pache L, Chang M, Khodabakhshi AH, Tanaseichuk O, Benner C, Chanda SK. 2019. Metascape provides a biologist-oriented resource for the analysis of systems-level datasets. Nat Commun 10:1523. https://doi.org/10.1038/s41467-019-09234-6.
60. Wang YQ, Song FH, Zhu JW, Zhang SS, Yang YD, Chen TT, Tang BX, Dong LL, Ding N, Zhang Q, Bai ZX, Dong XN, Chen HX, Sun MY, Zhai S, Sun YB, Yu L, Lan L, Xiao JF, Fang XD, Lei HX, Zhang Z, Zhao WM. 2017. GSA: Genome Sequence Archive. Genomics Proteomics Bioinformatics 15:14–18. https://doi.org/10.1016/j.gpb.2017.01.001.
61. CNCB-NGDC Members and Partners. 2021. Database resources of the National Genomics Data Center, China National Center for Bioinformation in 2021. Nucleic Acids Res 49:D18–D28. https://doi.org/10.1093/nar/gkaa1022.